Transient response of a projectile in gun launch simulation using lagrangian and ale methods[1]

Ala Tabiei[2]
Department of Aerospace Engineering & Engineering Mechanics
University of Cincinnati, Cincinnati, OH 45221-0070
ATabiei@aol.com
&
Mostafiz R. Chowdhury
U.S. Army Research Laboratory
2800 Powder Mill Rd
Adelphi, MD 20783-1145
Mchowdbury@arl.army.mil
&
N. Aquelet, M. Souli
Université de Lille, Laboratoire de Mécanique de Lille
Bd Paul Langevin Villeneuve d'Ascq 59655 France
nicolas_aquelet@yahoo.fr, mahmed.souli@univ-lille1.fr

ABSTRACT

This paper describes the usefulness of Lagrangian and arbitrary Lagrangian/Eulerian (ALE) methods in simulating the gun launch dynamics of a generic artillery component subjected to launch simulation in an air gun test. Lagrangian and ALE methods are used to simulate the impact mitigation environment in which the kinetic energy of a projectile is absorbed by the crushing of aluminum honeycomb mitigator. In order to solve the problem due to high impact penetration, a new fluid structure coupling algorithm is developed and implemented in LS-DYNA, a three dimensional FEM code. The fluid structure coupling algorithm used in this paper combined with ALE formulation for the aluminum honeycomb mitigator allows to solve problems for which the contact algorithm in the Lagrangian calculation fails due to high mesh distortion. The numerical method used for the fluid and fluid structure coupling is discussed. A new coupling method is used in order to prevent mesh distortion. Issues related to the effectiveness of these methods in simulating a high degree of distortion of Aluminum honeycomb mitigator with the commonly used material models (metallic honeycomb and crushable foam) are discussed. Both computational methods lead to the same prediction for the deceleration of the test projectile and are able to simulate the behavior of the projectile. Good agreement between the test results and the predicted projectile response is achieved via the presented models and the methods employed.

Keywords: Fluid/Structure Interaction, ALE method, honeycomb impact, air gun launch simulation

[1] Approved for public release; distribution is unlimited.
[2] Author to whom correspondence should be addressed

1. INTRODUCTION

An air gun test provides an efficient and effective launch simulation platform in which the shock phenomena in a real gun test are replicated in a controlled environment. The primary focus of such an air gun mitigation test is to simulate a transient shock environment that the test projectile is anticipated to encounter in an actual field test. Proper simulation of the gun launch environment via an air gun test requires a thorough understanding of the dynamics of the physical energy-absorbing interfacing components that regulate its shock environment. An analytical model in this regard could play a vital role in facilitating design and preparation of an effective air gun test. The ability to numerically simulate the dynamic response of the test projectile will allow the physical operating parameters of the air gun test environment to be tuned to achieve the specific dynamic profile for which the projectile has been tested. This methodology requires the development of a predictive model of responses of the test projectile. This paper presents the development of a finite-element (FE) model to simulate the dynamic impact response of a generic artillery component mounted on a given projectile during gun launch simulation in an air gun test.

Several LS-DYNA models of a generic test article fired in a 101.6-mm (4-in.) air gun chamber are developed in this study. Control test data for a test item mounted on a projectile are used for model validation and correlation. Analytical simulation of the air gun launch environment requires the modeling of an event in which the test object mounted on a projectile is launched and decelerated when it crushes an aluminum (Al) honeycomb mitigator in the recovery chamber. As a secondary energy-absorbing device, a momentum exchange mass (MEM) is used at the retrieving end. Two formulations are used in the simulations using explicit finite-difference methods. These included the Lagrangian and the arbitrary Lagrangian/Eulerian (ALE) formulations. Benson [1] reviews the basic explicit methods for solving transient, large deformation problems in solid mechanics.

During the crush simulation, the Al honeycomb mitigator undergoes significant deformation that could render a severely unstable Lagrangian simulation. For this reason, an ALE simulation is also considered. The Eulerian method is more suitable for problems involved in severe mesh distortion. The Lagrangian method, on the other hand, is limited in how much an element can deform. The Lagrangian method is easy to set up and visualize since the material point moves with the mesh. However, the Eulerian method is more difficult to set up and the mesh is stationary so that material points are advected from one element to the next. The Eulerian method allows new free surfaces to be created in a natural manner. An ALE method is a combination of Lagrangian and Eulerian formulations in which the parts that endure very large deformation such as those involving material flow are modeled with the Eulerian approach.

Two material formulations are used for simulating the Al honeycomb mitigator behavior with the Lagrangian method. These included honeycomb and crushable foam material models. The honeycomb material model simulates an anisotropic crushable behavior of a fully uncoupled system. The crushable foam material model, on the other hand, simulates an isotropic crushable behavior of a coupled system. This isotropic foam model crushes one dimensionally with a Poisson's ratio that is essentially zero. Most of the Al honeycomb material in the air gun simulation is crushed axially. Therefore, the crushable foam model is considered to be appropriate for simulating crushing behavior of an Al mitigator in the air gun test. The honeycomb material model formulation requires stress versus logarithmic strain relationship. Stress versus volumetric strain relationship is used to formulate the crushable foam material model. Only the crushable foam material model is used in the ALE method. The effectiveness of these two material models, along with the applicability of Lagrangian and ALE methods, are described next.

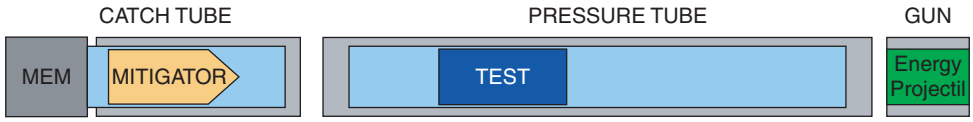

Figure 1 Schematic of an air gun test setup.

2. AIR GUN TEST DESCRIPTIONS

A schematic diagram for a typical air gun test setup is shown in Figure 1. The test setup consists of a stationary gun barrel, a projectile, and a dual energy-absorbing mechanism consisting of a mitigator and a MEM positioned at the recovery end. In a typical air gun mitigation test, the projectile carrying the artillery components to be tested is launched to impact an Al honeycomb mitigator at the recovery chamber. Upon impact with the mitigator, the kinetic energy of the projectile is lessened as the mitigator crushes. The crushed mitigator in turn exchanges its momentum with a MEM, a secondary energy-absorbing device, abutting its rear end.

A pre-shot arrangement of the dual energy-absorbing devices in an air gun retrieving chamber is shown in Figure 2. As seen in the figure, the mitigator is stationed inside the split catch tube at the start of the test. Four 12.7-mm (0.5-in.) diameter, 4340 steel tie rods (two each side of the isle; see Figure 2) are used to fasten the top half of the split catch tube with the stationary bottom half shown in the figure. The striking end of the 0.6087-gm/cm^3 (38-pcf) Al honeycomb mitigator was fashioned to form two sharp wedges. The 7075-T6 Al mitigator was 256.54 mm (10.1 in.) long, including a wedge depth of 38.1 mm (1.5 in.), 98.30 mm (3.87 in.) in diameter, and weighed about 1,110 gm. With two such wedges at the striking end, the mitigator tends to crush evenly across its face. The length of the wedges also determines the projectile's deceleration profile during the impact. The MEM at the recovery end weighed about 31,300 gm. A post-shot relative position for the physical apparatus is shown in Figure 3. As seen in this figure, upon hitting its target, the projectile remains trapped in the catch tube, the mitigator crushes, and the MEM displaces. A post-test configuration of the mitigator shows that the striking end of the mitigator solidifies more than its remote end.

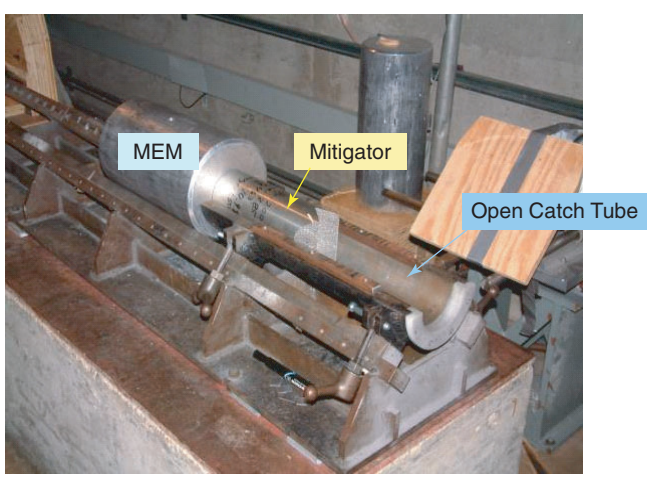

Figure 2 A pre-shot arrangement in the 4-inch air gun test.

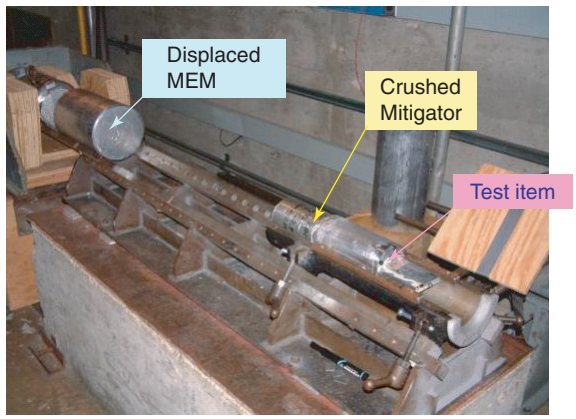

Figure 3 A post-shot configuration of interacting components in a 4-inch air gun test.

A test projectile consisting of a rectangular Al plate (101.0 mm [4 9 in.] × 76.2 mm [3 in.] × 12.7 mm [0.5 in.]) mounted on the top of an on-board recorder (OBR) case (152.4 mm [6 in.] in length, 101.09 mm [3.98 in.] in outer diameter with a thickness of 12.7 mm [0.5 in.]) was especially prepared for FE verification. The projectile including the OBR carrier and a rectangular plate mounted on its top weighed about 3,250 gm. In this test projectile, OBR records the data and the plate is the test item representing a simulated projectile component that could be used in an actual air gun test.

Figure 4 shows the test projectile and the instrument locations for which the data were recorded via an on-board 12-bit, 4-channel high shock analog recorder placed inside the OBR case. Two accelerometers and two strain gauges were mounted on the test item. The analog

Figure 4 An instrumented test projectile.

recorder was shock isolated inside the canister by the suspension of the device over glass beads and the canister being densely packed once the top mount had been assembled. An isolated packaging arrangement was needed to ensure survival of the OBR.

3. MATERIAL MODELS

One of the most difficult aspects of this investigation was to define the material properties that would represent the physical behavior of the Al honeycomb mitigator used in the air gun test. In this investigation, no test was conducted for characterizing mitigator properties. Therefore, the authors had to depend on the data available in the open literature. The crush test results available in reference [2] were used to construct the material model. As shown in Figure 5, three distinct features characterize the honeycomb mitigator's load-carrying behavior. These features included a linear elastic tendency until initial crushing, typical volumetric crush, and final phase of hardening to full compaction. Almost all energy absorption is done in the volumetric crush zone. Initial spikes at the end of linear behavior are typical in the Al honeycomb resistance profile, which can be eliminated by the crushing of the mitigator's striking edge. The fluctuation of strength during volumetric crushing, as seen in the figure, may have resulted from instability because of buckling of honeycomb cells.

The two material models considered here are honeycomb and crushable foam material formulations. The formulations of the two material models are described next.

3.1. HONEYCOMB MATERIAL MODEL

This material model is suited to model metallic honeycomb [3, 4, 5]. The behavior before compaction is orthotropic where the components of the stress tensor are uncoupled, i.e., a component of strain will generate resistance in the local a-direction with no coupling to the local *b* and *c* directions. The elastic modulii (E) vary (see Eqn. (1)) from their initial values to the fully compacted values linearly with the relative volume:

$$\begin{aligned} E_{aa} &= E_{aau} + \beta(E - E_{aau}) & G_{ab} &= G_{abu} + \beta(G - G_{abu}) \\ E_{bb} &= E_{bbu} + \beta(E - E_{bbu}) & G_{bc} &= G_{bcu} + \beta(G - G_{bcu}) \\ E_{cc} &= E_{ccu} + \beta(E - E_{ccu}) & G_{ca} &= G_{cau} + \beta(G - G_{cau}) \end{aligned} \tag{1}$$

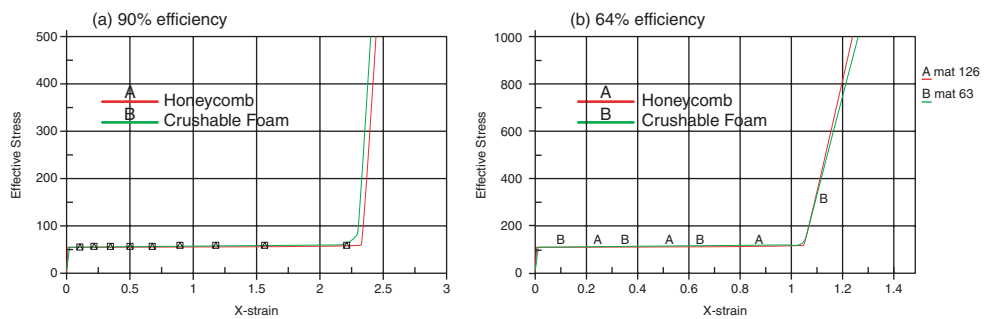

Figure 5 Simulated stress-strain curves using two materials models, 90% and 64% compaction (stress is in N/mm^2).

in which

$$\beta = \max\left[\min\left(\frac{1-V}{1-V_f}, 1\right), 0\right] \tag{2}$$

and G is the elastic shear modulus for the fully compacted honeycomb material:

$$G = \frac{E}{2(1+\nu)} \tag{3}$$

The relative volume, V, is defined as the ratio of the current volume over the initial volume, and typically, $V = 1$ at the beginning of a calculation.

At the beginning of the stress revision, each element's stresses and strain rates are transformed into the local element coordinate system. For the uncompacted material, the stress components are revised (see Eqn.(4)) by the elastic interpolated modulii according to the following:

$$\begin{aligned} \sigma_{aa}^{n+1trial} &= \sigma_{aa}^{n} + E_{aa}\Delta\varepsilon_{aa} & \sigma_{ab}^{n+1trial} &= \sigma_{ab}^{n} + E_{ab}\Delta\varepsilon_{ab} \\ \sigma_{bb}^{n+1trial} &= \sigma_{bb}^{n} + E_{bb}\Delta\varepsilon_{bb} & \sigma_{bc}^{n+1trial} &= \sigma_{bc}^{n} + E_{bc}\Delta\varepsilon_{bc} \\ \sigma_{cc}^{n+1trial} &= \sigma_{cc}^{n} + E_{cc}\Delta\varepsilon_{cc} & \sigma_{ca}^{n+1trial} &= \sigma_{ca}^{n} + E_{ca}\Delta\varepsilon_{ca} \end{aligned} \tag{4}$$

We then independently check each component of the revised stresses to ensure that they do not exceed the permissible values determined from the load curves; e.g., if

$$\left|\sigma_{ij}^{n+1trial}\right| > \lambda\sigma_{ij}(\varepsilon_{ij}) \tag{5}$$

then

$$\sigma_{ij}^{n+1} = \sigma_{ij}(\varepsilon_{ij})\frac{\lambda\sigma_{ij}^{n+1trial}}{\left|\sigma_{ij}^{n+1trial}\right|} \tag{6}$$

The components of $\sigma_{ij}(\varepsilon_{ij})$ are defined by load curves.

The material model requires the stress versus logarithmic strain input for material characterization [6]. The relation between the engineering strain, e and the logarithmic strain, ε is given by $\varepsilon = ln(1+e) = ln\left(\left|\frac{L}{L_o}\right|\right)$ in which the engineering strain, e, is defined by the equation $e = \frac{L-L_o}{L_o} = \frac{L}{L_o} - 1 = \frac{\Delta L}{L_o}$.

For instance, if the efficiency of the honeycomb material is 90%, the material final length is only 10% of its initial length. The logarithmic strain in this case is $\varepsilon = \left|ln\left(\left|\frac{0.1}{1.0}\right|\right)\right| = 2.3026$.

3.2. CRUSHABLE FOAM MATERIAL MODEL

This material model is suited for modeling crushable foam [3, 4, 5]. This isotropic foam model crushes one dimensionally with a Poisson's ratio that is essentially zero. In the implementation, we assume that Young's modulus is constant and revise the stress, assuming elastic behavior (see Eqn. (7)).

$$\sigma_{ij}^{n+1trial} = \sigma_{ij}^{n} + E\dot{\varepsilon}_{ij}^{n+1/2}\Delta t^{n+1/2} \tag{7}$$

The magnitudes of the principal values σ_i^{trial}, i = 1,3 are then checked to see if the yield stress σ_y is exceeded; if so, they are scaled back to the yield surface so that, if

$$\sigma_y < \left|\sigma_i^{trial}\right| \tag{8}$$

then

$$\sigma_{ij}^{n+1} = \sigma_y \frac{\sigma_i^{trial}}{\left|\sigma_i^{trial}\right|} \tag{9}$$

After the principal values are scaled, the stress tensor is transformed back into the global system.

The material model requires the stress versus volumetric strain relationship [6]. The volumetric strain ε_v is defined as $\varepsilon_v = 1 - \frac{V}{V_o} = 1 - \frac{AL}{A_o L_o}$.

Since we can assume that the crushable foam is crushed under a very small Poisson's ratio, the initial cross-sectional area is the same as the final one. Therefore, in this case the volumetric strain can be simplified as $\varepsilon_v = 1 - \frac{L}{L_o}$.

3.3. MATERIAL PARAMETERS

Parameters of interest for the material model include crush strength, crush efficiency (volumetric strain that initiates the hardening), hardening modulus, and strain rate enhancement attributable to increase in impact velocity. In this investigation, a stress scale factor (relative increase in strength because of impact velocity) suggested by Bitzer [7], which ranges from 1.2 to 1.5, is used because of the unavailability of high strain rate-dependent experimental data.

In order to verify the validity of the materials models, an FE model was developed to simulate the compression test reported in literature [2]. The displacement control is used in the simulation. The simulated stress-strain curves for 90% and 64% compaction are compared in Figure 5 for both material models. This figure clearly identifies three distinct features in load-carrying behavior of honeycomb materials. These features included linear elastic tendency until initial crushing, typical volumetric crush, and final phase of hardening to full compaction. Almost all energy absorption is done in the volumetric crush zone. Initial spikes at the end of linear behavior are typical in Al honeycomb resistance profile, which can be eliminated by the crushing of the mitigator's striking edge.

The mean values and the overall trends in the simulated curve closely match the test data presented by Lu and Hutchinson [2]. A 90% efficiency means that the final length is only 10% of its initial length. Predicted crushing strain, thus for 90% efficiency (~2.5 mm/mm) is greater than the 64% case (~1 mm/mm) as indicated in Figure 5. A simulation is also performed for the static and rate sensitive cases. Results indicate that the rate-sensitive stress is about two times the static stress [8]. This simulation testifies to the effectiveness of the proposed material models in simulating the mean load-displacement relationship of the Al honeycomb mitigator. This material model, however, disregards the strength fluctuation during volumetric crush as evidenced in the physical test data shown in reference [2].

4. ARBITRARY LAGRANGE EULER FORMULATION

4.1. ALE DESCRIPTION

Lagrangian approaches easily model problems, in which interfaces between different materials are present. However, if an analysis for complex geometry is required, the distortion of the Lagrangian mesh involves to use many re-meshing steps in order to continue the calculation. Another method to use is the Eulerian formulation. This change from a Lagrangian to an Eulerian formulation, however, introduces two problems. The first problem is the interface tracking [9] and the second problem is the advection phase or advection of fluid material across element boundaries.

To solve these problems, an explicit finite element method for the Lagrangian phase and a finite volume method (flux method) for the advection phase are used. Please refer to the LS-DYNA theoretical manual [3] for a full description of the explicit finite element method.

The advection phase has been added to the LS-DYNA code extending the range of applications that can be used with the ALE formulation [10, 11, 12, 13]. Current industrial applications include: sloshing involving a 'free surface' [14], and slamming problems [15], which are high velocity impact problems where the target is modeled as a fluid material, thus providing a more realistic representation of the impact event by capturing large deformations.

An ALE formulation contains both pure Lagrangian and pure Eulerian formulations [10]. The pure Lagrangian description is the approach that: the mesh moves with the material, making it easy to track interfaces and to apply boundary conditions. Using an Eulerian description, the mesh remains fixed while the material passes through it. Interfaces and boundary conditions are difficult to track using this approach; however, mesh distortion is not a problem because the mesh never changes. In solid mechanics a pure Eulerian formulation is not useful because it can handle only a single material in an element, while an ALE formulation is assumed to be capable of handling more than one material in an element [13].

In the ALE description, an arbitrary referential coordinate is introduced in addition to the Lagrangian and Eulerian coordinates [10]. The material derivative with respect to the reference coordinate can be described as Eqn. (10). Thus substituting the relationship between the material time derivative and the reference configuration time derivative derives the ALE equations,

$$\frac{\partial f(X_i,t)}{\partial t} = \frac{\partial f(x_i,t)}{\partial t} + w_i \frac{\partial f(x_i,t)}{\partial x_i} \tag{10}$$

where X_i is the Lagrangian coordinate, x_i the Eulerian coordinate, w_i is the relative velocity. Let denote by v the velocity of the material and by u the velocity of the mesh. In order to simplify the equations we introduce the relative velocity $w = v - u$. Thus the governing equations for the ALE formulation are the mass, momentum and energy equations given by the following equations:

$$\frac{\partial \rho}{\partial t} = -\rho \frac{\partial v_i}{\partial x_i} - w_i \frac{\partial \rho}{\partial x_i} \tag{11}$$

$$\rho \frac{\partial v_i}{\partial t} = \sigma_{ij,j} + \rho b_i - \rho w_i \frac{\partial v_i}{\partial x_i} \tag{12}$$

$$\rho \frac{\partial e}{\partial t} = \sigma_{ij} v_{i,j} + \rho b_i v_i - \rho w_j \frac{\partial e}{\partial x_j} \tag{13}$$

where ρ is the material density, b_i, the body forces, e, the internal energy.
The stress tensor σ_{ij} is described as follows:

$$\sigma_{ij} = -p\delta_{ij} + \mu(v_{i,j} + v_{j,i}).$$

where δ_{ij} is Kronecker's delta function, p, the pressure field, μ, the dynamic viscosity. The strong form of the problem governing Newtonian fluid flow in a fixed domain consists of the governing equations and suitable initial and boundary conditions (see Eqn. (14), Eqn. (15), Eqn. (16) and Eqn. (17)). Thus the last equations are solved with the following boundary conditions and initial conditions:

$$v_i = U_i^0 \qquad \text{on } \Gamma_1 \tag{14}$$

$$\sigma_{ij} n_j = 0 \qquad \text{on } \Gamma_2 \tag{15}$$

where

$$\Gamma_1 \cup \Gamma_2 = \Gamma, \Gamma_1 \cap \Gamma_2 = 0 \tag{16}$$

Γ is the whole boundary of the calculation domain, and Γ_1 and Γ_2 are partial boundaries of Γ. The superscript means prescribed value, n_i is the outward unit normal vector on the boundary. The velocity field is assumed as known at $t = 0$ in the whole domain Ω.

$$v_i(x_i, 0) = 0 \tag{17}$$

The equations governing the fluid problem are the ALE description of the Navier-Stokes equations because the term in the relative velocity in Eqn. (11) and Eqn. (12) is usually referred to as the advective term, and accounts for the transport of the material past the mesh. It is the additional term in the equations that makes solving the ALE equations much more difficult numerically than the Lagrangian equations, where the relative velocity is zero. Note that the Eulerian equations are derived by assuming that the velocity of the reference configuration is zero and that the relative velocity between the material and the reference configuration is therefore the material velocity.

There are two ways to implement the ALE equations, and they correspond to the two approaches taken in implementing the Eulerian viewpoint in fluid mechanics. The first way solves the fully coupled equations for computational fluid mechanics; this approach used by different authors can handle only a single material in an element [10]. The alternative approach is referred to as an operator split in the literature, where the calculation, for each time step is divided into two phases. First a Lagrangian phase is performed, in which the mesh moves with the material, in this phase the changes in velocity an internal energy due to the internal and external forces are calculated. The equilibrium equations are:

$$\rho \frac{\partial v_i}{\partial t} = \sigma_{ij,j} + \rho b_i, \tag{18}$$

$$\rho \frac{\partial e}{\partial t} = \sigma_{ij} v_{i,j} + \rho b_i v_i. \tag{19}$$

In the Lagrangian phase, mass is automatically conserved, since no material flows across the element boundaries.

In the second phase, the advection phase, transport of mass, internal energy and momentum across cell boundaries are computed; this may be thought of as remapping the displaced mesh at the Lagrangian phase back to its original for an Eulerian formulation, or arbitrary position for an ALE formulation.

From a discretization point of view, one point integration is used for efficiency and to eliminate locking [13]. The zero energy modes are controlled with an hourglass viscosity [16]. A shock viscosity, with linear and quadratic terms, is used to resolve the shock wave; a pressure term is added to the pressure in the energy equation. The resolution is advanced in time with central difference method, which provides a second order accuracy in time, and which leads to a staggered time for displacement and velocity, thus the displacement is defined at time $t^n = n \cdot \Delta t$, and velocity at time $t^{n-1/2} = \left(n \cdot - \frac{1}{2}\right)\Delta t$. For each node, the velocity and displacement are updated as follow:

$$v_i^{n+1/2} = v_i^{n-1/2} + \frac{\Delta t}{M}\left(F_i - \int B^t \bar{\bar{\sigma}} dx\right) \tag{20}$$

$$\vec{x}^{n+1} = \vec{x}^{n} + \Delta t \cdot \vec{v}^{n+1/2} \tag{21}$$

where F_i is the external vector force associated with body forces and boundary conditions, M is the diagonal mass matrix, and B^t is the discrete gradient operator, $\bar{\bar{\sigma}}$ is the total stress, including the pressure and deviatoric parts, computed from the constitutive material model. The time step size Δt, is limited by the Courant stability condition, which may be expressed as:

$$\Delta t \le \frac{l}{Q + (Q^2 + c^2)^{1/2}} \quad \text{with} \quad \begin{array}{ll} Q = C_1 c + C_2 |\mathrm{div}(\vec{v})| & \text{if } \mathrm{div}(\vec{v}) < 0 \\ Q = 0 & \text{if } \mathrm{div}(\vec{v}) \le 0 \end{array} \tag{22}$$

$\mathrm{div}(\vec{v}) = \frac{\partial v_1}{\partial x_1} + \frac{\partial v_2}{\partial x_2} + \frac{\partial v_3}{\partial x_3}$ is the volumetric strain rate of the material defined using the velocity vector $\vec{v} = (v_1, v_2, v_3)$. The volumetric strain rate of the element can be expressed using element volume, $\mathrm{div}(\vec{v}) = \frac{\Delta V}{V \cdot \Delta t}$ where V is element volume and ΔV the volume change for the time step. l is the characteristic length of the element, Q is a term derived from the shock viscosity, C_1 and C_2 are the coefficients for the linear and quadratic terms of the shock viscosity. The Q term introduced in the equation is positive for compression and zero for tension, when c is the speed of sound through the material in the element. For a solid material, the speed of sound is:

$$c^2 = \frac{\frac{4}{3}G + k}{\rho_0} \tag{23}$$

$$k = \rho_0 \frac{\partial P}{\partial \rho} + \frac{P}{\rho}\frac{\partial P}{\partial e} \tag{24}$$

where ρ_0 is the initial material density, G is the shear modulus, and $P(\rho, e)$ is the equation of state. In k, the second term on the right hand side accounts for the stiffening effect due to the increase of internal energy as the material compressed. For fluid material the viscosity is

ignored in the calculation of the speed of sound. For sloshing tank problems the pressure is much greater than the deviatoric components stress due the fluid viscosity, and the deviatoric stress is sometimes ignored.

4.2. VOF METHOD

In the impact problem, a VOF method (Volume Of Fluid) is used, this formulation allows an element to be partially filled, a volume fraction of the material, V_f, is defined for each element, thus the element, which allows the material to flow through a fixed mesh, where the empty element have a zero volume fraction, and the partially filled element have a volume fraction between the values 0. and 1. The VOF is attractive for solving a broad range of non-linear problems in fluid and solid mechanics, because it permits arbitrary large deformations and allows free surfaces to evolve. The Lagrangian phase of the VOF method is easily implemented in an explicit ALE finite element method. Before advection, special treatment for the partially voided element is needed. For an element that is partially filled, $V_f < 1$. The total stress by $\overline{\overline{\sigma}}$ is weighted by volume fraction.

$$\overline{\overline{\sigma}}_f = \overline{\overline{\sigma}} \cdot V_f \tag{25}$$

For voided elements, the stress is zero. In the computational process, the elements loop goes only through elements that are not totally voided. For free surface problems, the elements that are partially filled are the elements where $V_f < 1$, and define the free surface.

4.3. STRESS EQUILIBRIUM AND INTERFACE TRACKING

After the Lagrangian phase is performed, either the stress tensor, pressure and deviatoric stress should be equilibrated, but most of the mixture theories equilibrate only pressure [13], the equilibration pressure is a non-linear problem, which is complex and expensive to solve. Skipping the stress equilibrium phase is assuming equal strain rate for both materials and is incorrect. For most of the problems, the linear distribution based on volume fraction of the volumetric strain during the Lagrangian phase also leads to incorrect results. The volume distribution should be scaled by the bulk compression of the two materials in the element. In an element containing air and water, the air is highly compressible. So air will absorb most of the volumetric strain. Thus by assuming equal strain rate or volumetric strain scaled on the volume fraction of the element, the water is forced to accept the same amount of strain as the air, and will undergo artificial high stresses.

There are several methods for treating the free surface in a multi-material problem; the common one is the MAC method, which involves Eulerian flow calculation and Lagrangian particle movement. The velocity of the markers is found by first locating the cell containing the particle and taking the average velocities of the cell nodes (the averaging is based on the finite element particles in the cell). The particle cells have small inertia and tend to follow the material deformation. However, the MAC method becomes complicated if the interfaces become highly distorted or if the geometry is complex.

Another possible way of tracking interfaces is the use of the volume fractions of the elements, or the Young method [17]. The Young method is developed to track an interface in elements containing two materials for two-dimensional problems. This method is adapted in this paper for the three dimensional problems. In this method, the material layout is described solely by the volume fraction of materials in the element. Specifically, a straight line using the SLIC technique (Simple Linear Interface Calculation) of Woodward and Collela [18] approximates the interface in the cell. Interfaces are initially drawn parallel to the element faces. Then nodal volume fraction is computed at each node based on the fraction volumes of elements that share the same node. This

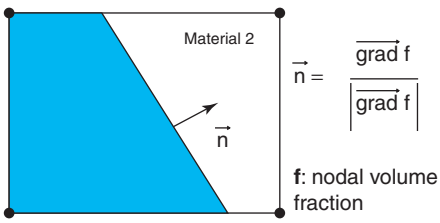

Figure 6 Interface oriented by the normal $\vec{n}$ in an Eulerian cell.

volume fraction intern determines the slope of the material interface inside the element. The position of the interface (see Figure 6) is then adjusted so that it divides the element into two volumes, which correctly matches the element volume fraction.

The interface position is used to calculate the volume of the fluid flowing across cell sides. As the X-advection, Y-advection and Z-advection are calculated in separate steps, it is sufficient to consider the flow across one side only. The interface calculation prevents advection of very small fluxes between partially filled and empty elements. Instead fluid flow is transported from 'filled' element to 'empty' element and this change in volume will be monitored and used to 'fill-up' the element or increase its volume fraction.

4.4. ADVECTION

In the second phase, the transport of mass, momentum and internal energy across the element boundaries is computed. This phase may be thought of as a 're-mapping' phase. The displaced mesh from the Lagrangian phase is remapped into the initial mesh for an Eulerian formulation, or an arbitrary mesh for an ALE formulation.

In this advection phase, we solve a hyperbolic problem, or a transport problem, where the variables are density, momentum per unit volume and internal energy per unit volume. Details of the numerical method used to solve the equations are described in detail in [17] and [19], where first order Donor Cell method and second order Van Leer algorithm [20] are used. As an example, the equation for mass conservation is:

$$\frac{\partial \rho}{\partial t} + \vec{\nabla} \cdot (\rho \vec{v}) = 0 \tag{26}$$

It is not the goal of this paper to describe the different algorithms used to solve Eqn. (26), these algorithms have already been described in detail by Benson [19] and Souli et al. [21]. We will focus on the 'staggered' mesh used for the momentum advection, described by Benson [19].

The advected momentum is used for the computation of the new nodal velocities. To prevent distribution of momentum from nodes to elements during the advection and from elements to nodes during nodal velocity calculations, the momentum advection is done only through the nodes. This procedure requires a staggered mesh. A mesh is staggered with respect to the original mesh so that the original mesh centroids become the new nodes. Yaqui [22] developed the first code to construct a staggered mesh (see Figure 7) for the momentum advection, and the basic idea is still in common use.

A cell centered advection algorithm is applied to the staggered mesh for the momentum advection. The data necessary for the advection algorithm are the cell volume before and after the Lagrangian phase, velocities of nodal masses and fluxes between cells. All the data are readily except for the fluxes. The new flux values on the staggered mesh are defined using a

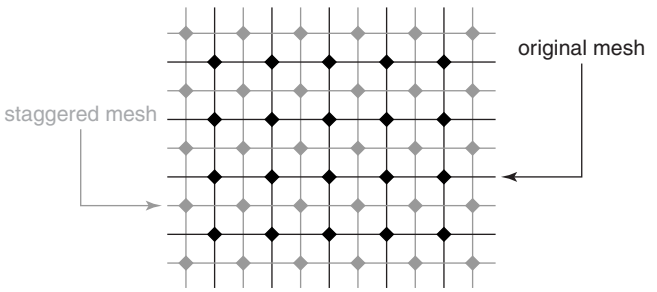

Figure 7 Staggered mesh and original mesh.

regular distribution of the fluxes from the original mesh element faces to the element faces on the staggered mesh.

4.5. EULER-LAGRANGE COUPLING

Most of impact problems are solved using a classical Lagrangian formulation with contact algorithm [23] and element erosion based on plastic strain or pressure failure, in order to prevent high mesh distortion. These algorithms are not mass conservative and sometime it is not possible to adjust the plastic strain failure for erosion. The new algorithm used to solve the problem is not based on element erosion, but a new material, air or void, occupies partially or fully the cell, the air material is defined as a fluid material using fluid constitutive model with an equation of state which computes the pressure in the element using the density and internal energy. For problems using void material, the void is assumed as zero stress material. In the new coupling, mitigator and air materials are modeled using an Eulerian or fixed mesh, a Lagrangian formulation is used for the impactor. The Lagrangian mesh moves and deforms inside the Eulerian fixed mesh. The coupling interface is defined through the material interface between mitigator and air materials, as shown in figure 17. Coupling forces are computed using a penalty method based on spring stiffness [24, 25]. Unlike the penalty contact used between two Lagrangian meshes, the penalty coupling is used between an Eulerian grid which models the mitigator and air materials and a Lagrangian mesh which models the impactor. Penalty coupling allows material to flow through the mesh and around a structure but not through a structure. Penalty forces are calculated proportionally to the penetration velocity and depth to behave like a spring system. The coupling method has been used successfully for different applications, where contact algorithms fail, due to high mesh distortion at the contact interface; high impact problems with 8 nodes hex elements are usually very difficult to simulate using contact, the coupling method is an alternative since mesh distortion is prevented using a fixed mesh for the target material. To illustrate the coupling used in this paper, let us consider a rigid structure with initial velocity is impacting a fluid, as shown in Figure 8, to clarify the mesh used for the problem, only the fluid and Air mesh is illustrated, the structure mesh, not shown on the figure, moves freely on the fixed ALE mesh. A constitutive model with an equation of state is used for the water considered as a target material, the air material occupies partially or completely the elements that will be eroded in a classical Lagrangian calculation. In the new coupling formulation the ALE mesh (water and air) is fixed and fluid material flows through the mesh. This formulation is very useful for high impact and penetration problems since mesh distortions, which cause the time step to decrease, and the problem to stop for negative volume. Nevertheless there are other problems related to the

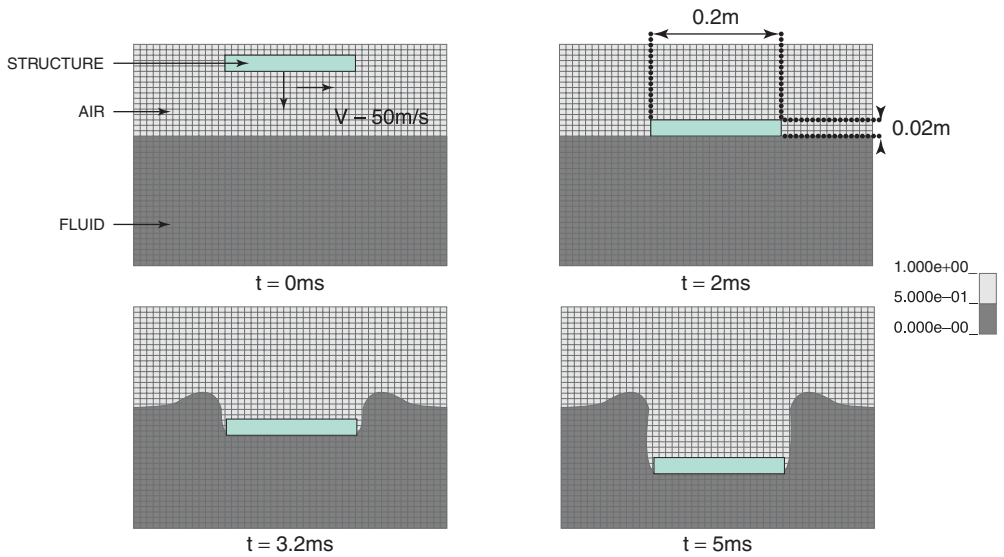

Figure 8 Impact of a plate on a free surface.

method, as to prevent fluid leakage through the structure. This is one of the difficulties we are facing using this method.

5. THE FINITE ELEMENT MODELS

5.1. LAGRANGIAN MODEL

The FE model of the Lagrangian test setup is depicted in Figure 9. The model consists of the catch tube (the wired mesh), the OBR (the brown mesh), the instrumented plate (the dark blue mesh), the MEM, (the yellow mesh), and four beam elements that represented the bolts connecting the two halves of the catch tubes. Upon modeling the OBR, no inner filler materials including the recording devices and the glass beads were included in the FE model.

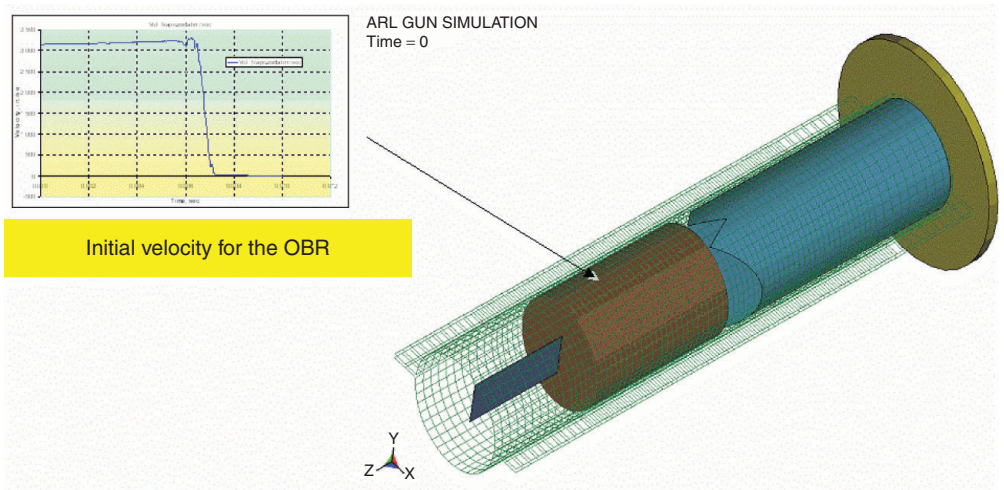

Figure 9 The Lagrangian finite element mesh.

We simulated the total mass of the instrumented OBR in the FE model by adjusting the density of the OBR canister. The analytical simulation of the impact starts with an initial input velocity for the projectile from the position shown in the figure.

The FE model consists of 118,842 nodes and 123,164 elements. There are 14,744 shell elements, 108,416 solid elements, and 4 beam elements in the model. Several contact surfaces are defined in this model. A contact surface is defined between the OBR and the mitigator, the OBR and the catch tube, the mitigator and the catch tube, and the mitigator and the MEM. The segment-based contact is used in this case, which proved to be more stable. Material models, honeycomb and crushable foam, are used in this model.

5.2. ALE MODEL

Since it is difficult to simulate very large deformation in the Lagrangian method easily, the ALE method is employed. The Lagrangian method requires significant expertise in the modeling of severe deformation. The ALE method, on the other hand, is more stable for such problems. The mesh model reported in this paper consisted of 69,578 node and 65,724 elements. There are 4,440 shell elements, 61,280 solid elements, and 4 beam elements in the model. The ALE FE model consists of the catch tube, the OBR (glass beads are not modeled as in Lagrangian case), the instrumented plate, and the MEM that is similar to the Lagrangian model. The mitigator, however, is modeled differently here. The mitigator is modeled with solid element formulation No. 12 in LS-DYNA. This element formulation is ALE and void. The mesh in this part does not distort, which is the case with Eulerian description of motion. The mitigator is surrounded by void elements. The void element is there for the possibility of the mitigator material flow. Upon deformation, the mitigator material can flow outside of the mitigator mesh. Once this happens, the mitigator material can flow into the void elements. The solid elements of the mitigator and void have node-to-node correspondence at the boundaries. Figure 10 depicts a section cut through the middle of the mesh. The blue mesh represents the mitigator honeycomb and the red mesh is the surrounding void.

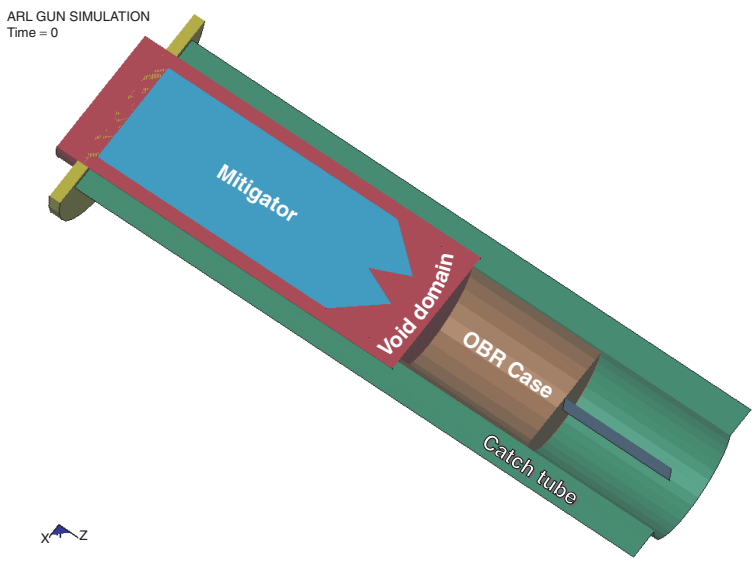

Figure 10 Section cut of ALE model.

The integration time step in an ALE simulation is smaller than a Lagrangian simulation for the same mesh size. The explicit time integration time step in the Lagrangian method, in general, is a function of the smallest element's characteristic length and material properties. In the ALE method, in addition to the above, it is also a function of mesh velocity. Therefore, the integration time step in the ALE method is smaller than the Lagrangian method.

6. SIMULATION RESULTS

The simulations are performed on a 1.7-MHz laptop computer and also independently on an Army Research Laboratory Major Shared Resource Center's SGI Origin 2000 system. The impact event is about 2 milliseconds (ms). The contact of the OBR with the mitigator is about 1 ms only. The CPU time with the laptop for the Lagrangian simulation is about 4 hours. The Eulerian simulation takes about 16 hours to completion even though the number of elements is about half those of the Lagrangian simulation. The impact velocity in both models is taken as 83,566 mm/sec (3,290 in./sec.) We obtained the initial velocity by double integrating the recorded accelerometer data from the actual test shot. The three fundamental units used here are millimeter (mm), second (sec), and metric ton for the length, time, and mass, respectively. Results of the two simulations are presented next.

6.1. LAGRANGIAN SIMULATIONS

6.1.1. Honeycomb Material Model

The strain rate effect must be included in such a simulation since the material exhibits strain rate sensitivity. However, since experimental data for the used honeycomb material under high strain rate are not available, a multiplier scales the stresses. The range of stress scale factor used is between 1.2 and 1.5 for this material model [7]. The honeycomb material reported in reference [2] has an efficiency of 64 to 90%. The 64% efficiency (or compaction) predicted a stiffer response than the 90% compaction. Figure 11 shows the difference in predictions of the

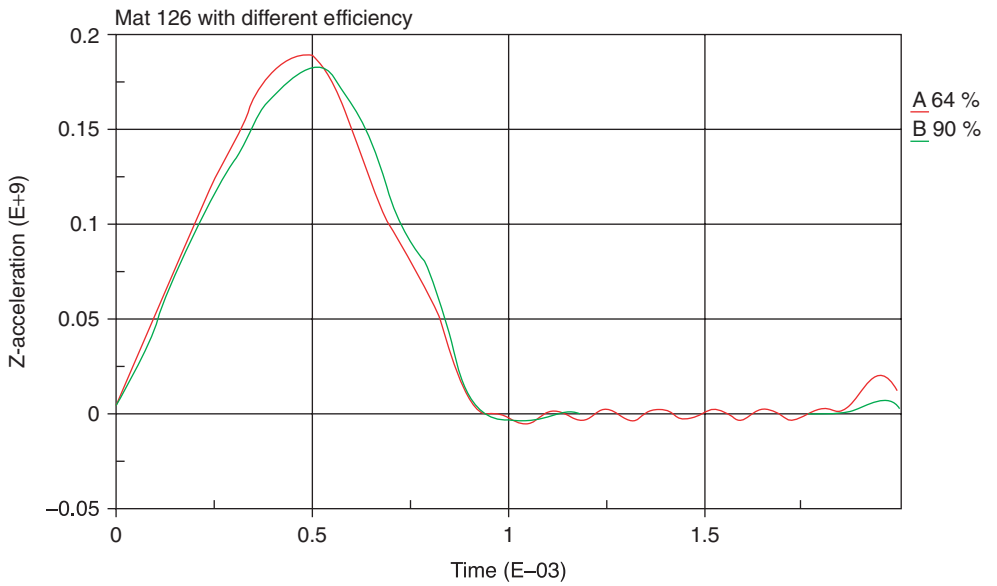

Figure 11 Acceleration of the top of the OBR for two different efficiencies.

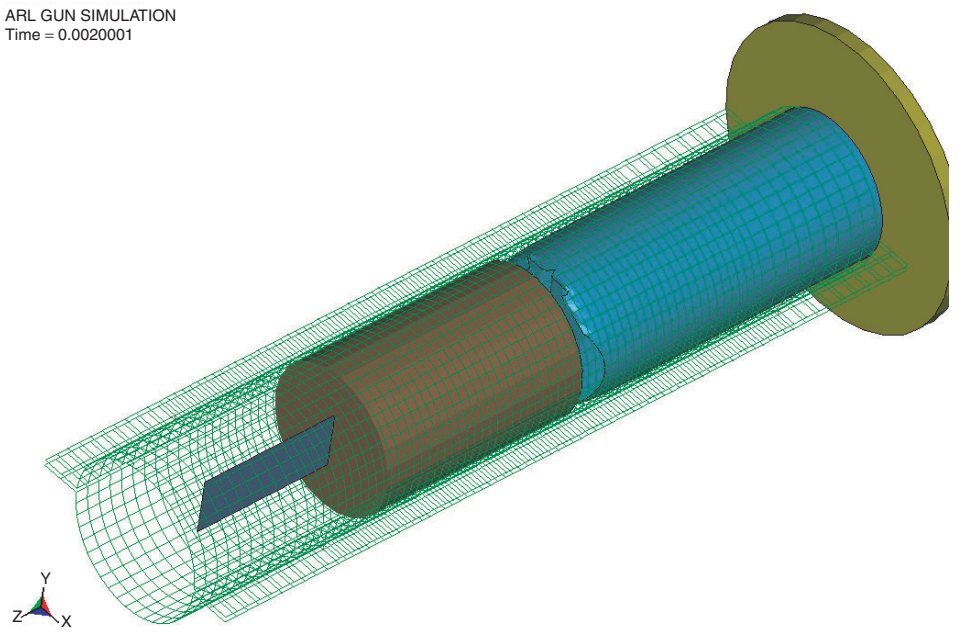

Figure 12 Impact simulation with the honeycomb material model.

two efficiencies. Figure 12 shows the impacted geometry and a view of the impacted geometry of the air gun launch simulation. Figure 13 depicts the energy balance as predicted by the simulation. One can see that the energy is conserved in this simulation, which is an indication of numerical stability of the model. The hourglass energy and contact energy (not shown here) are much smaller than the internal energy as desired in a stable impact simulation.

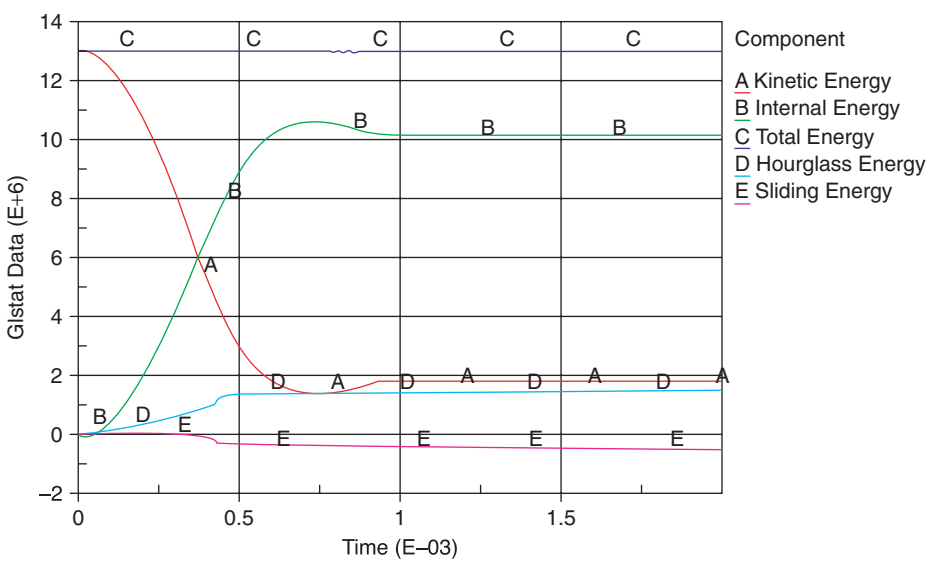

Figure 13 Energy balance, honeycomb material model.

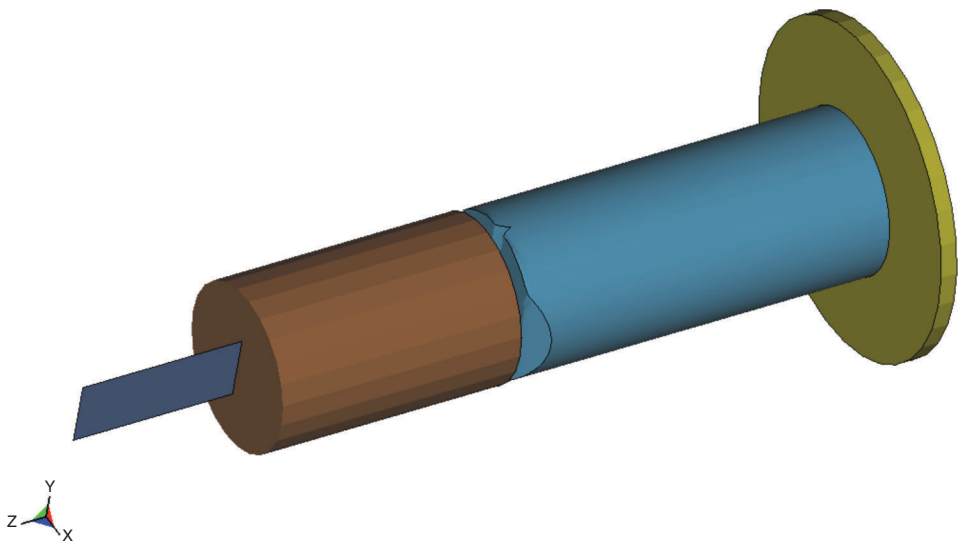

Figure 14 Crushed mitigator, crushable foam model.

Crushable Foam Material Model

The CPU time for the simulation with this material model is about the same as for the honeycomb material model discussed before. The crushed mitigator is shown in Figure 14. A stress scale factor of 1.5 is used to account for the strain rate sensitivity. The qualitative difference between the simulations with honeycomb and crushable foam models was insignificant. Figure 15 and 16 shows the displacement of the MEM and filtered acceleration of the top of the OBR for both material models respectively. The magnitude of the acceleration for the two materials is about the same. However, there is some difference in the

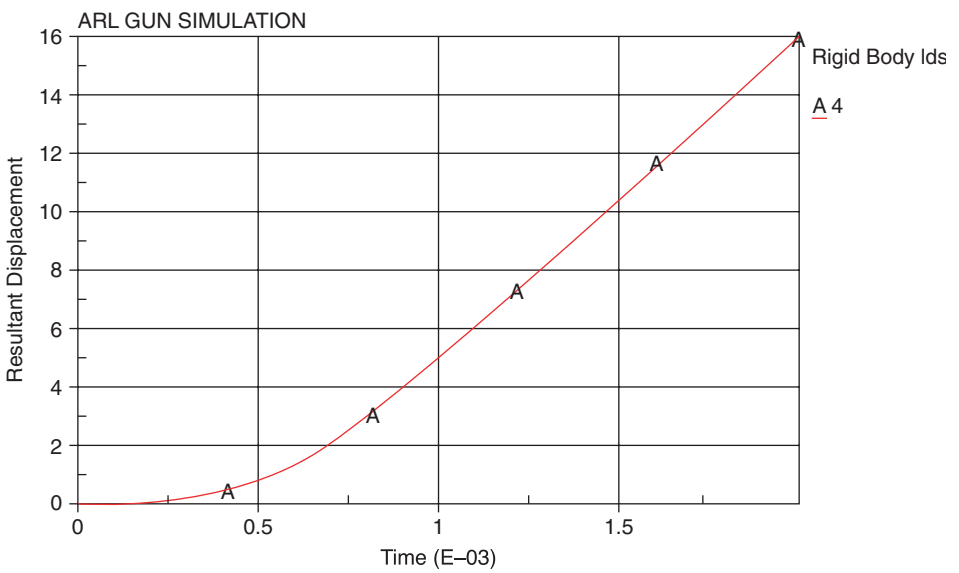

Figure 15 Displacement of the MEM, honeycomb material model.

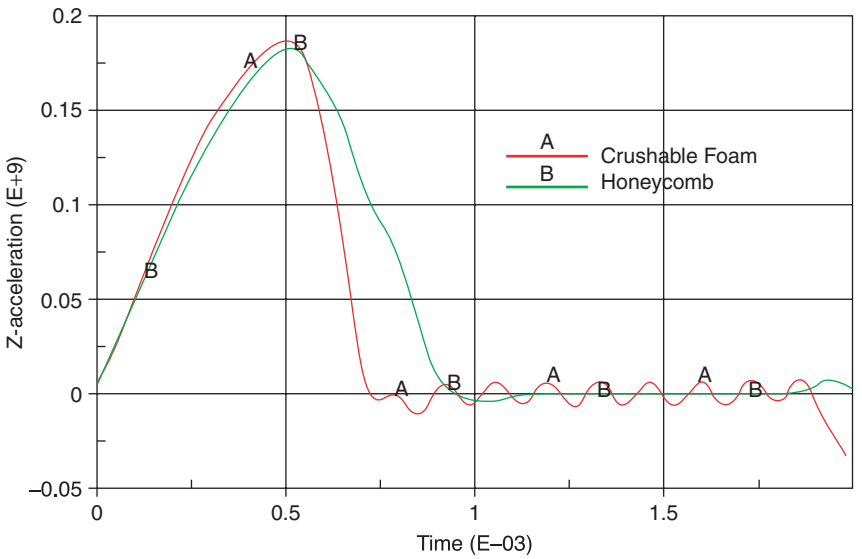

Figure 16 Acceleration (in mm per sec^2) of the top of the OBR with honeycomb and crushable foam models.

duration of the pulse. This difference is attributed to the differences in the formulation of the two material models. The honeycomb model is an orthotropic material, which assumes that stress components are fully decoupled. Straining of the material in the local material axis in one direction causes stress in that direction only. However, the crushable foam is an isotropic material model and the stress components are not decoupled.

6.2. ALE SIMULATION

The mesh is fixed in an ALE simulation. In this situation, one can look at the volume fraction of the material. The volume fraction is equal to 1 when the element is filled with the material. A volume fraction of less than 1 means that only part of the element is filled with the material. The volume fraction of the mitigator material at the end of the simulation is depicted in Figure 17. One can observe that the Eulerian mesh has not moved; however, the material has passed from one element to next, indicating material flow and deformation.

A comparison of the prediction of the acceleration of the top of the OBR via the Lagrangian and ALE methods is shown in Figure 18. These data are filtered with a low pass filter with a cut-off frequency of 2500 Hz. A small difference is observed in the magnitude of the peak acceleration. This difference, however, can be neglected and assumed to be the numerical error difference between the two methods.

7. MODEL VALIDATION: SIMULATION VERSUS EXPERIMENT

The simulation results are compared with experiments qualitatively and quantitatively. Qualitatively, the deformation of the mitigator looks the same in the simulation and experiment. The experimental final crushed length of the mitigator is reported as 210.0 mm (8.27 in.). The simulated final crushed length of the mitigator is predicted to be 226.0 mm (8.90 in.) —A difference of about 7% from the actual crushed length.

The quantitative validation consists of comparing the acceleration data from simulation and experiment for the locations shown in Figure 4. The locations of nodes for which the data were extracted are at the same locality as in the test setup.

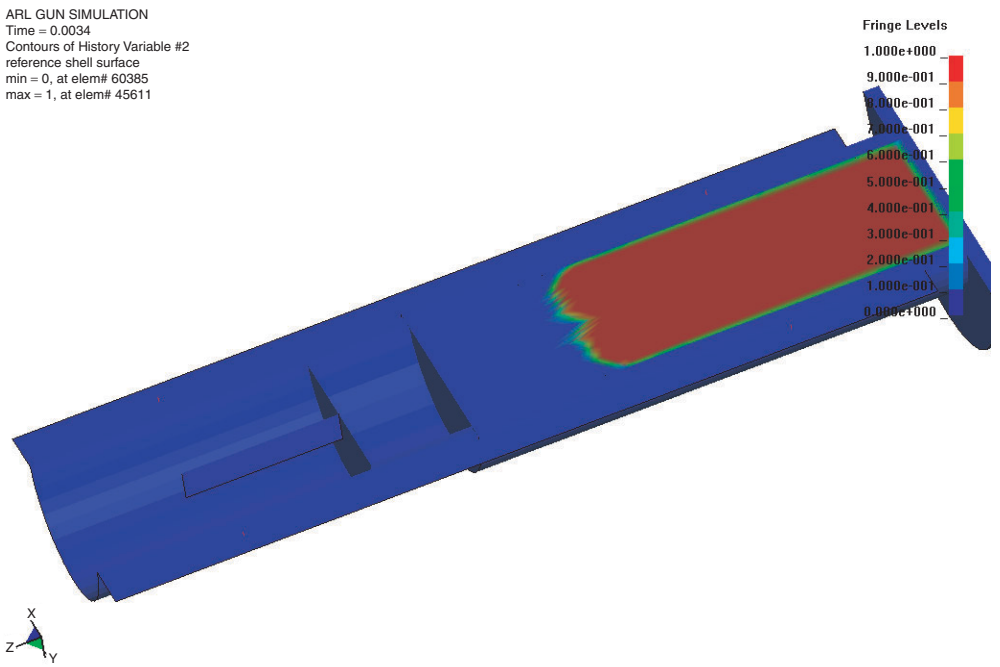

Figure 17 Volume fraction of the mitigator at the end of the simulation.

For comparison purposes, the simulation results and the experimental results are filtered with low pass cut-off frequencies of 7,000 Hz and 2,500 Hz, respectively. The simulations and the experiment's acceleration of the top of the OBR for both filtrations are shown in Figures 19 and 20. Figure 19 shows a relatively good agreement between the predicted and test acceleration responses with the honeycomb material model when a stress scaled factor

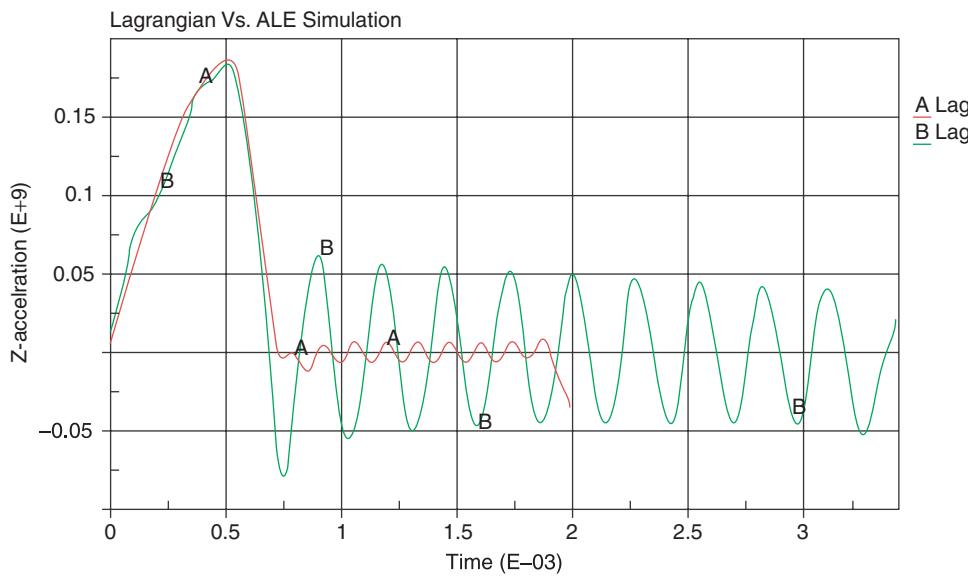

Figure 18 Acceleration (in mm per sec^2) of the top of the OBR filtered at 2500 Hz for both the Lagrangian and ALE simulations.

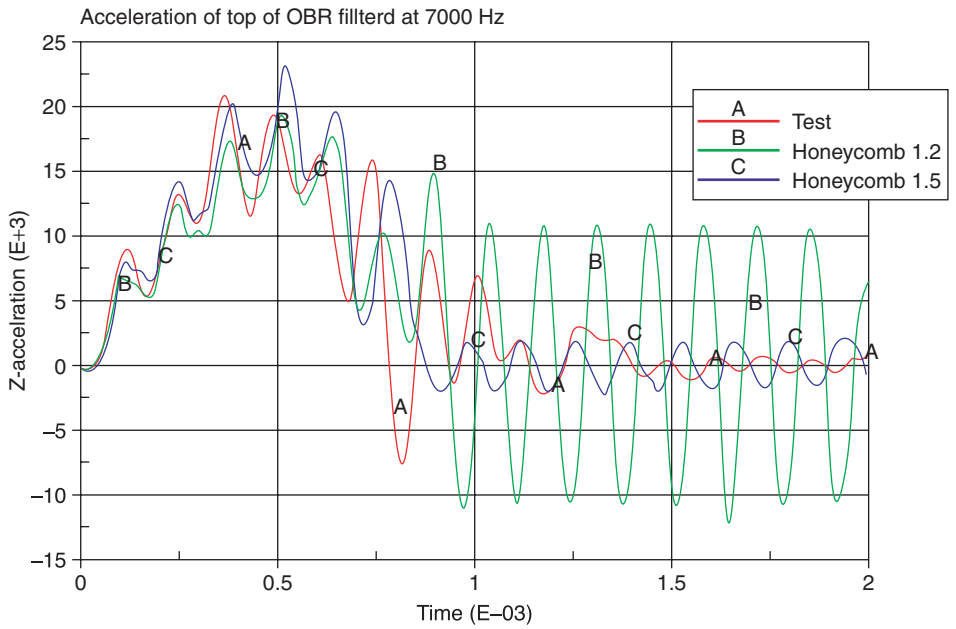

Figure 19 Simulation versus experiment, acceleration (in g's) of top of OBR filtered at 7000 Hz.

of 1.5 was used in the analysis. A higher stress scale factor (1.5 instead of 1.2) has significantly attenuated the free vibration, as indicated in Figure 19. Good prediction is observed from the simulation as compared to experiment, particularly for the 2500-Hz cut-off frequency. Figure 20 compares several runs for the simulation. Two predictions are presented for the honeycomb material model with two different stress factors (1.2 and 1.5). One can observe that when the stress is scaled by 1.2, the peak acceleration is under-predicted. When the stress is scaled by 1.5, the peak acceleration is over-predicted. Figure 20 also shows the prediction of acceleration with the crushable foam material model. In this case, the stress is also scaled by 1.5.

8. CONCLUSIONS

Lagrangian and ALE methods are developed to simulate the air gun launch environment in which a test object mounted on a projectile is fired through the air gun and decelerated by the crushing of an Al honeycomb mitigator which impacts the MEM before being stopped at the retrieving end. The Lagrangian method is simpler to set up, post process, and requires less computational time. However, it requires significant expertise in the FE model to make the simulation numerically stable. This is because of the significant large deformation of the mitigator. On the other hand, the ALE method is more difficult to set up, post process, and requires much more CPU time. However, the ALE simulation is more suitable for very large deformation problems such as those involving material flow. Both computational methods lead to the same prediction for the acceleration of the OBR.

Material models, honeycomb and crushable foam, lead to reasonable predictions and are able to simulate the behavior of the mitigator. The strain rate sensitivity must be accounted for in these simulations. If no strain rate effect is included, the peak acceleration of the OBR is under predicted. In the presented simulation, instead of activating the rate effect in the

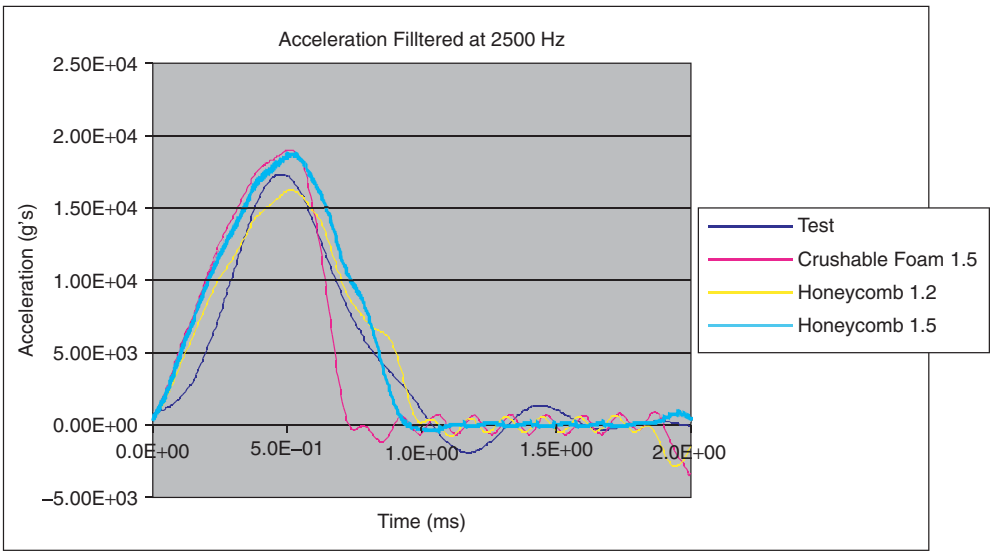

Figure 20 Simulation versus experiment, acceleration of top of OBR filtered at 2500 Hz.

material models, the stress is scaled by values between 1.2 and 1.5. This will have the same effect as if the rate effect were activated in the material model.

Good prediction of the period and peak acceleration of the OBR is achieved with the presented models and the methods employed. A similar FE modeling technique can be used for such problems with confidence that the code will aid in the prediction of the proper response of any instrument mounted on the OBR.

ACKNOWLEDGMENTS

The analytical work presented here was accomplished under a contract (TCN: 02-125) with the Scientific Services Program (STAS) of U.S. Army Research Office (ARO), Research Triangle Park, North Carolina. We greatly appreciate the services of ARO in facilitating the contract and the support of U.S. Army Research Laboratory in allowing us to publish the document.

REFERENCES

[1] Benson, D.J. (1991), "Computational Methods in Lagrangian and Eulerian hydrocodes", *Computer Methods in Applied Mechanics and Engineering*. **99,** 235–394.

[2] Lu, W. and Hinnerichs, T. (2001), "Crush of High Density Aluminum Honeycombs", Proceedings of the International Mechanical Engineering Congress and Exposition, November 11–16.

[3] Hallquist, J.O. (1998), 'LS-DYNA Theoretical Manual', LSTC, Livermore, CA.

[4] Hallquist, J.O. (1998), 'LS-DYNA Users Manual, Vol. 1', LSTC, Livermore, CA.

[5] Hallquist, J.O. (1998), 'LS-DYNA Users Manual, Vol. 2', LSTC, Livermore, CA.

[6] Tabiei, A. (1999–2002), "Advance LS-DYNA Lecture Notes", Cincinnati, OH.

[7] Bitzer, T. (1997), Honeycomb Technology, Champman & Hall, London, UK.

[8] Chowdhury, M.R. and Tabiei, A. (2003), "Development of An Air Gun Simulation Model Using LS-DYNA", Final Report, TCN 02–125, U.S. Army Research Office, RTP, NC.

[9] Nakayama, T., Mori, M. (1996), "An Eulerian Finite Element method for time-dependent free-surface problems in hydrodynamics", *International Journal for Numerical Methods in Fluids*. **22**(3), 175–194.

[10] Hughes, T. J. R., Liu, W. K., and Zimmerman, T. K., (1981), "Lagrangian Eulerian finite element formulation for viscous flows", *J. Comput. Methods Appl. Mech. Engrg*. 21 329–349.

[11] Donea, J., (1983), "Arbitrary Lagrangian-Eulerian Finite Element Methods, Computational methods for Transient Analysis", T. Belytschko and T.J.R. Hughes, ed. Elsevier Sciences Publishers, B.V. 473–513.

[12] Benson, D J., (1989), "An efficient, accurate, simple ALE method for nonlinear finite element programs", Computational Methods In Applied Mechanics and Engineering 1989 **72**, 305–350.

[13] Benson, D.J. (1997), "A mixture Theory for Contact in Multi-Material Eulerian Formulations", *Computer Methods in Applied Mech. and Eng*. **140**, 59–86.

[14] Aquelet, N., Souli, M., Gabrys, J. and Olovsson, L. (2003) "A new ALE formulation for sloshing analysis", *Structural Engineering and Mechanics*. **16**(4), 423–440.

[15] Aquelet, N., Souli, M. and Olovsson, L. (2005) "Euler-Lagrange coupling with damping effects: Application to slamming problems", Comput. Methods Appl. Mech. Engrg., accepted.

[16] Flanagan, D.P. and Belytschko, T. (1981), "A Uniform Strain Hexahedron and Quadrilateral and Orthogonal Hourglass Control", *Int. J. Numer. Meths, Eng*. **17**, 679–706.

[17] Young, D.L. (1982) "Time-dependent multi-material flow with large fluid distortion", Numerical Methods for Fluids Dynamics, Ed. K. W. Morton and M.J. Baines, Academic Press, New-York.

[18] Woodward, P.R., and Collela, P. (1982), "The numerical simulation of two-dimensional fluid flow with strong shocks", Lawrence Livermore National Laboratory. UCRL-86952.

[19] Benson, D.J. (1992), "Momentum Advection on a Staggered Mesh", *Journal of Computational Physics*. **100**(1), 143–162.

[20] Van Leer, B. (1977), "Towards the Ultimate Conservative Difference Scheme. IV. A New Approach to Numerical Convection", *Journal of Computational Physics*. **23**, 276–299.

[21] Souli, M., Ouahsine, A., Lewin, L. (2000), "ALE formulation for fluid-structure interaction problems", *Computer Methods in Applied Mech. and Eng*. **190**, 659–675.

[22] Amsden, A. A., and Hirt, C. W. (1973), "YAQUI: An Arbitrary Lagrangian-Eulerian Computer Program for Fluid Flow at All Speeds", Los Alamos Scientific Laboratory, LA-5100.

[23] Zhong, Z.H., (1993), "Finite Element Procedures for Contact-impact Problems", Oxford University Press, Oxford.

[24] Belytschko, T., Neal, M.O., (1989), "Contact-impact by the pinball algorithm with penalty, projection, and Lagrangian methods", in: Proceedings of the Symposium on Computational Techniques for Impact, Penetration, and Performation of Solids AMD, **vol.103**, ASME, New York, NY, pp. 97–140.

[25] Belytschko, T., Liu, W.K., Moran, B., (2000), "Nonlinear Finite Elements for Continua and Structures", John Wiley & Sons, Ltd.